

Article

Deboronation-Induced Ratiometric Emission Variations of Terphenyl-Based *Closo-o*-Carboranyl Compounds: Applications to Fluoride-Sensing

Hyunhee So [†], Min Sik Mun [†], Mingi Kim [†], Jea Ho Kim, Ji Hye Lee , Hyonseok Hwang , Duk Keun An ^{*} and Kang Mun Lee ^{*} 

Department of Chemistry, Institute for Molecular Science and Fusion Technology, Kangwon National University, Chuncheon 24341, Korea; shh6353@naver.com (H.S.); bbcisgj2002@kangwon.ac.kr (M.S.M.); kmg6523@kangwon.ac.kr (M.K.); syoil12@daum.net (J.H.K.); jhlee81@kangwon.ac.kr (J.H.L.); hhwang@kangwon.ac.kr (H.H.)

^{*} Correspondence: dkan@kangwon.ac.kr (D.K.A.); kangmunlee@kangwon.ac.kr (K.M.L.);

Tel.: +82-33-250-8494 (D.K.A.); +82-33-250-8499 (K.M.L.)

[†] These authors contributed equally to the work.

Academic Editor: Ashok Kakkar

Received: 25 April 2020; Accepted: 21 May 2020; Published: 21 May 2020



Abstract: *Closo-o*-carboranyl compounds bearing the *ortho*-type perfectly distorted or planar terphenyl rings (*closo-DT* and *closo-PT*, respectively) and their *nido*-derivatives (*nido-DT* and *nido-PT*, respectively) were synthesized and fully characterized using multinuclear NMR spectroscopy and elemental analysis. Although the emission spectra of both *closo*-compounds exhibited intriguing emission patterns in solution at 298 and 77 K, in the film state, *closo-DT* mainly exhibited a π - π^* local excitation (LE)-based emission in the high-energy region, whereas *closo-PT* produced an intense emission in the low-energy region corresponding to an intramolecular charge transfer (ICT) transition. In particular, the positive solvatochromic effect of *closo-PT* and theoretical calculation results at the first excited (S_1) optimized structure of both *closo*-compounds strongly suggest that these dual-emissive bands at the high- and low-energy can be assigned to each π - π^* LE and ICT transition. Interestingly, both the *nido*-compounds, *nido-DT* and *nido-PT*, exhibited the only LE-based emission in solution at 298 K due to the anionic character of the *nido-o*-carborane cages, which cannot cause the ICT transitions. The specific emissive features of *nido*-compounds indicate that the emissive color of *closo-PT* in solution at 298 K is completely different from that of *nido-PT*. As a result, the deboronation of *closo-PT* upon exposure to increasing concentrations of fluoride anion exhibits a dramatic ratiometric color change from orange to deep blue via turn-off of the ICT-based emission. Consequently, the color change response of the luminescence by the alternation of the intrinsic electronic transitions via deboronation as well as the structural feature of terphenyl rings indicates the potential of the developed *closo-o*-carboranyl compounds that exhibit the intense ICT-based emission, as naked-eye-detectable chemodosimeters for fluoride ion sensing.

Keywords: *closo-o*-carborane; *nido-o*-carborane; intramolecular charge transfer; deboronation; color change

1. Introduction

Closo-ortho-carboranes (1,2-dicarba-*closo-o*-dodecaboranes, *o*-1,2- $C_2B_{10}H_{12}$) are well-known boron-cluster components of three-dimensional (3D) icosahedral analogs. Recently, *closo-ortho*-carboranes have attracted significant attention as new molecular scaffolds of steric and electronic substituents for luminescent organic and organometallic compounds due to their unique

photophysical properties and reasonable thermal and electrochemical stabilities originating from the *o*-carborane unit [1–28]. These electronic features are imparted by the electron-withdrawing properties of the carbon atoms, and the high polarizability of the σ -aromaticity of the organic and organometallic luminophores that comprise the *o*-carborane moiety. These characteristics lead to the formation of electronic donor-acceptor dyad systems that induce intrinsic intramolecular charge transfer (ICT) transitions between the π -conjugated aromatic groups and the *o*-carborane cage [29–53]. Such ICT characteristics can induce unique luminescence behavior in various *o*-carborane-based organic luminophores [29–70]. Interestingly, such an intramolecular radiative mechanism activated by the ICT transitions in the *o*-carboranyl luminophores has been found amenable to modifications via variations to the structure of the *o*-carborane cages or appended aryl groups [32,43–53,70] and their molecular geometries [66–69]. Furthermore, the direct control of the ICT-based emission in the *closo-o*-carboranyl compounds involves the conversion of *closo-o*-carboranes to *nido-o*-species (*o*-1,2-C₂B₉H₁₂[−], one boron atom removed analog of the *closo-o*-carborane cage) by reaction with nucleophilic anions. This powerful process can cause dramatic changes in the inherent electronic environment because of the strong electron-donating property of *nido-o*-carboranes [71], leading to the alteration of their luminescent features [72–78]. For example, Carter et al. reported a fluorene-based dimer bearing an *o*-carborane, which exhibited a visible fluorescence change (orange to bright blue) by degradation to the *nido*-species [73]. Furthermore, Núñez et al. reported photoluminescent *closo*- and *nido*-di-carboranyl and tetra-carboranyl derivatives, which possessed intrinsic ICT electronic transitions and demonstrated differences in the emission band maxima of the two species [75]. We recently reported polyolefins bearing pendant *o*-carborane moieties that exhibit strong blue emissions in the solid state. Notably, the observed emissions disappeared after degradation of the carborane cage upon reaction with hydroxyl ions [76]. Additionally, 1,3,5-tris-(*closo-o*-carboranyl-methyl)benzene displayed ratiometric emissive color change via deboronation to the corresponding *nido-o*-species [77]. The degradation of the *closo-o*-carborane–triarylborane dyad to the *nido-o*-carboranyl compound exhibited a turn-on fluorescence response toward fluorides [78]. Thus, these *closo-o*-carboranyl derivatives exhibited great potential as polymeric or single-molecular chemodosimeters for sensing nucleophilic anions.

On the basis of inducing significant changes in the electronic properties through the conversion of *closo-o*-carborane to its anionic *nido-o*-species, we sought to investigate in detail the impact of the deboronation of the *closo-o*-carboranyl compounds on their ICT-based emission. For this study, we designed two simple terphenyl-based *o*-carboranyl compounds based on our previous results [69] (Figure 1). The first is 2',5'-dimethyl-1,1':4',1''-terphenyl-based *closo-o*-carborane (**DT**), with distorted *o*-terphenyl rings, which showed a weak ICT-based emission transition, and the second is 6,6,12,12-tetramethyl-6,12-dihydroindeno[1,2-*b*]fluorene-based *closo-o*-carboranyl compound (**PT**), with planar *o*-terphenyl rings, which possessed an intense emission from the ICT transition. Subsequently, the designed *closo-o*-compounds, as well as the *nido-o*-carboranyl compounds, were prepared and fully characterized. The comparison of the photophysical properties of these *closo*- and *nido*-compounds indicated that the deboronation of the *o*-carborane moiety and the structural feature of the appended terphenyl rings may deactivate the ICT transition and also quenching of the emission, thereby providing a novel method for fluoride sensing.

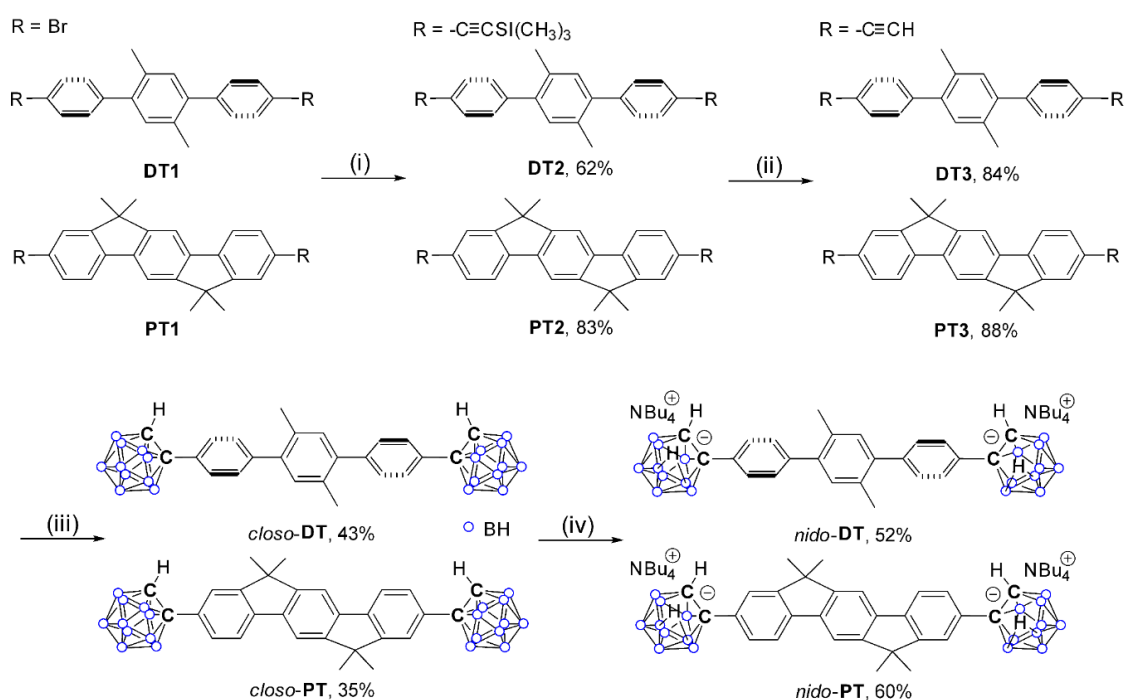


Figure 1. Synthetic routes to the terphenyl-based *closo*- and *nido*-*o*-carboranyl complexes, *closo*-**DT**, *closo*-**PT**, *nido*-**DT**, and *nido*-**PT**. Reaction conditions: (i) Ethynyltrimethylsilane, CuI, Pd(PPh₃)₂Cl₂, NEt₃/toluene, r.t., 24 h. (ii) K₂CO₃, methanol, r.t., 2 h. (iii) B₁₀H₁₄, Et₂S, toluene, 110 °C, 72 h. (iv) *n*-tetrabutylammonium fluoride (TBAF), THF, 60 °C, 2 h.

2. Results and Discussion

2.1. Synthesis and Characterization

The synthetic routes for the terphenyl-based *closo*-*o*- (*closo*-**DT** and *closo*-**PT**) and *nido*-*o*- (*nido*-**DT** and *nido*-**PT**) carboranyl compounds, where the *o*-carborane cages are substituted at both the ends by terphenyl moieties, are outlined in Figure 1. The Sonogashira coupling reaction between ethynyltrimethylsilane and the bromo-precursors **DT1** and **PT1** produced the ethynyltrimethylsilane-substituted terphenyl compounds **DT2** and **PT2**, respectively, in high yields (62% for **DT2** and 83% for **PT2**). The mild base (K₂CO₃)-mediated deprotection of the trimethylsilyl protecting groups of **DT2** and **PT2** furnished **DT3** and **PT3**, respectively, which were then subjected to decaborane (B₁₀H₁₄)-promoted cage-forming reactions in the presence of Et₂S (Figure 1) [79–81] to prepare the *closo*-*o*-carborane-substituted terphenyl compounds *closo*-**DT** and *closo*-**PT**, respectively. The dimethyl groups of *closo*-**PT** were introduced to achieve good solubility in a range of organic solvents. Subsequent treatment of *closo*-**DT** and *closo*-**PT** with excess *n*-tetrabutylammonium fluoride (NBu₄F, TBAF) in THF at 60 °C led to the conversion of the *closo*-carboranes to the *nido*-species; *nido*-**DT** is the (NBu₄)₂-salt of the *nido*-form of *closo*-**DT**, and *nido*-**PT** is the (NBu₄)₂-salt of the *nido*-form of *closo*-**PT** (Figure 1).

All of the prepared *closo*- and *nido*-*o*-carboranyl compounds were fully characterized using multinuclear (¹H{¹¹B}, ¹³C, and ¹¹B{¹H}) NMR spectroscopy (Figures S1–S12 in the Supplementary Material) and elemental analysis. The ¹H and ¹³C NMR spectra of *closo*-**DT** and *closo*-**PT** exhibited resonances corresponding to the terphenyl moieties. In addition, five broad singlet peaks were observed between −2 and −15 ppm in the ¹¹B{¹H} NMR spectra of both *closo*-**DT** and *closo*-**PT**, which confirmed the presence of the *closo*-*o*-carborane cage. Furthermore, signals were observed at ~78 and ~61 ppm in the ¹³C-NMR spectra, which were attributed to the two carbon atoms of the *closo*-*o*-carboranyl groups. Unlike the neutral *closo*-**DT** and *closo*-**PT**, the broad singlets (δ = −2.3 and −2.4 ppm) in the

$^1\text{H}\{^{11}\text{B}\}$ NMR spectra of both *nido-DT* and *nido-PT* are characteristic of the B–H–B bridge protons of *nido-o*-carborane moieties. The $^{11}\text{B}\{^1\text{H}\}$ NMR signals of *nido-DT* and *nido-PT* at δ ca. -8 to -37 ppm, which are shifted significantly upfield due to the anionic character of the *nido-o*-carboranes, clearly confirmed the presence of the *nido-o*-carboranyl boron atoms.

2.2. Photophysical Properties of the Closo- and Nido-o-Carboranyl Compounds

The photophysical properties of all terphenyl-based *closo*- and *nido-o*-carboranyl were investigated using UV/Vis absorption and photoluminescence (PL) spectroscopies (Figure 2 and Table 1). The *closo-o*-carboranyl compounds, *closo-DT* and *closo-PT*, displayed major absorption bands at $\lambda_{\text{abs}} = \sim 268$ and 336 nm, respectively, with structureless vibronic features. These bands were attributed to spin-allowed $\pi-\pi^*$ LE transitions of the central terphenylene groups [82] and typical ICT transitions between the *o*-carborane units and the central phenyl rings (see the time-dependent density functional theory (TD-DFT) results *vide infra*). Indeed, these ICT-based low-energy absorption bands were not present in the spectra of *nido-DT* and *nido-PT*, due to which those absorption spectra were slightly blue-shifted ($\lambda_{\text{abs}} = 254$ and 323 nm, respectively, Table 1) compared with those of the *closo*-compounds. These findings imply that the deboronation of the *o*-carborane cages in the *nido*-species quenches the ICT transitions involving the *o*-carborane unit.

To gain insight into the intrinsic photophysical properties of all *o*-carboranyl compounds, the emissive properties of *closo-o*-compounds were examined by PL under a variety of conditions, and further, the emissions of *nido-o*-compounds in THF at 298 K were investigated (Figure 2 and Table 1). Although the PL spectra of both *closo-DT* and *closo-PT* in THF exhibited intriguing emission patterns in all states upon excitation at 292 and 345 nm, respectively, the *closo-DT* emission was focused in the high-energy region centered at $\lambda_{\text{em}} = \sim 350$ nm, whereas *closo-PT* exhibited an intense low-energy emission in the 500 to 600 nm range, which tailed off at 650 nm. With reference to the results of the TD-DFT computational study (*vide infra*), this high-energy emission appears to originate from the $\pi-\pi^*$ LE transitions of the central terphenyl moieties. In contrast, the low-energy emission is closely associated with ICT transitions between the *o*-carborane cages and the terphenyl rings. Furthermore, the emission spectrum of *closo-DT* in THF at 298 K exhibited an intense emission in the high-energy region at $\lambda_{\text{em}} = 350$ nm due to $\pi-\pi^*$ LE transitions based on the central phenyl rings. The fact that the high-energy emission band of *closo-DT* was consistently maintained in a variety of solvents of different polarities ($\lambda_{\text{em}} = 349\text{--}350$ nm, Table 1 and Figure S14a in the Supplementary Material) and that the low-energy emission of *closo-PT* was dramatically altered (Table 1 and Figure S14b), strongly indicates that *closo-DT* and *closo-PT* exhibit LE- and ICT-based emissive characteristics, respectively. These intriguing features are clear evidence that the planarity of the terphenyl rings plays an important role in the alternation of the intramolecular electronic transitions as well as the corresponding radiative decay mechanism [69]. Moreover, *closo-DT* exhibited only a trace ICT-based emission in solution (THF solution at 298 K), and the PL spectra in the rigid state (THF at 77 K and in the film state, i.e., 5 wt% doped on poly(methyl methacrylate) (PMMA)) showed an enhanced low energy emission ($\lambda_{\text{em}} = 482$ nm in THF at 77 K and $\lambda_{\text{em}} = 492$ nm in the film) that tailed to 550 nm. The emission band for *closo-PT* around 500 nm was also significantly increased in the rigid state (THF at 77 K and in film), indicating that the electronic transition for both *closo*-compounds are governed by non-radiative process in solution state at 298 K. This behavior originates from the increased efficiency of the radiative decay associated with the ICT transition in the rigid molecular state, which restricts structural fluctuations such as C–C bond variations in the *o*-carborane cage [9,38,66–69]. In addition, the PL spectra of the two *nido-o*-compounds in THF at 298 K exhibited identical emission patterns in the high-energy region ($\lambda_{\text{em}} = 343$ nm for *nido-DT* and 390 nm for *nido-PT*, respectively) alone, and each spectrum of the *closo*-compounds corresponded to the terphenyl-centered $\pi-\pi^*$ LE transition. Accordingly, these phenomena demonstrate that the CT-based emission can be quenched by the anionic character of *nido-o*-carborane as well as the distortion of the terphenyl rings, which inhibits the ICT transitions. Such features suggest that *closo-o*-carboranyl compounds that exhibit the intense ICT-based emission,

such as *closo-PT*, can cause dramatic emission color changes via deboronation of the *o*-carborane cage, owing to the interruption of the ICT transition corresponding to the *o*-carborane and conservation of the LE transition. This phenomenon was verified by spectral changes in the emission of *closo-PT* in the presence of TBAF (*vide infra*).

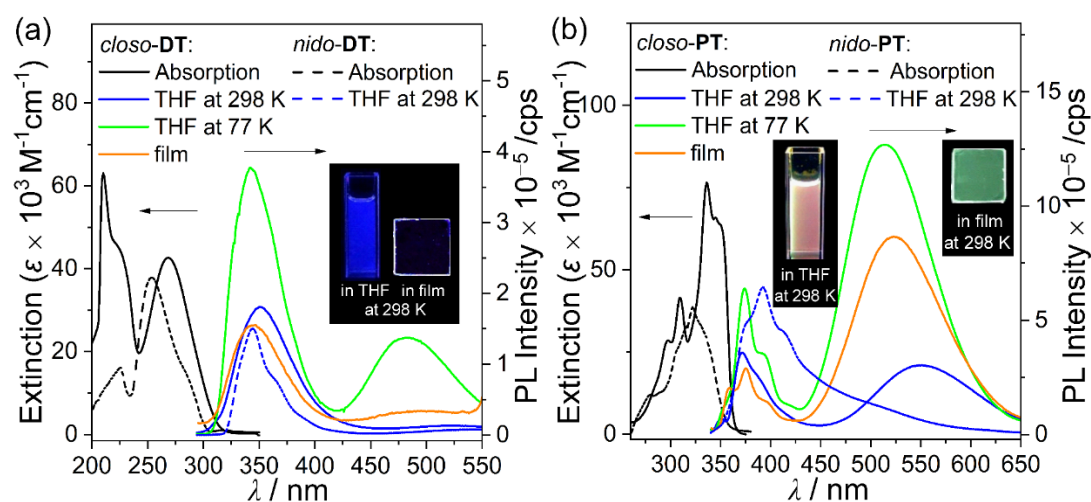


Figure 2. UV-Vis absorption and photoluminescence (PL) spectra for (a) *closo*- and *nido*-DT ($\lambda_{\text{ex}} = 292$ nm) and (b) *closo*- and *nido*-PT ($\lambda_{\text{ex}} = 345$ nm). Black-solid: absorption spectra in THF (30 μM) for *closo*-species. Black-dash: absorption spectra in THF (30 μM) for *nido*-species. Blue-solid: PL spectra in THF (30 μM) at 298 K for *closo*-species. Blue-dash: PL spectra in THF (30 μM) at 298 K for *nido*-species. Green-solid: PL spectra in THF (30 μM) at 77 K for *closo*-species. Orange-solid: PL spectra of the films (5 wt% doped on PMMA) at 298 K for *closo*-species. Inset figures show the emission color in each state of *closo*-species under irradiation by a hand-held UV lamp ($\lambda_{\text{ex}} = 295$ nm for *closo*-DT and 365 nm for *closo*-PT).

Table 1. Absorption and emission data for terphenyl-based *o*-carboranyl compounds.

Compound	$\lambda_{\text{abs}}^1/\text{nm}$ ($\epsilon \times 10^{-3} \text{ M}^{-1} \text{ cm}^{-1}$)	$\lambda_{\text{ex}}/\text{nm}$	$\lambda_{\text{em}}/\text{nm}$				
			Tol ²	THF ²	DCM ²	77 K ¹	Film ³
<i>closo</i> -DT	268 (42.6)	292	349	350	349	343, 482	345, 492(sh)
<i>nido</i> -DT	254 (37.8)	292	-	343	-	-	-
<i>closo</i> -PT	336 (84.8)	345	376, 521	374, 549	375, 560	374, 514	375, 524
<i>nido</i> -PT	323 (38.2)	345	-	390	-	-	-

¹ $c = 30$ μM in THF. ² $c = 30$ μM , observed at 298 K. ³ Measured in the film state (5 wt% doped on PMMA) at 298 K.

2.3. Computational Chemistry and Orbital Analyses for *Closo*-*o*-Carboranyl Compounds

To elucidate the nature of the electronic transitions and to analyze the orbitals of *closo*-DT and *closo*-PT, their S_0 - and S_1 -optimized structures were subjected to TD-DFT calculations using the B3LYP functional (Figure 3 and Table 2). To include the effects of the THF solvent [83,84], a conductor-like polarizable continuum model was chosen. The computational data for the S_0 state showed that HOMO \rightarrow LUMO transitions are the major lowest-energy electronic transitions in both *closo*-*o*-carboranyl compounds. The HOMO of each compound is entirely localized on the central terphenyl group (>96%; Tables S2 and S4 in the Supplementary Material), whereas the orbital contribution of the *o*-carborane unit to each LUMO is slightly higher, at >16%. These results indicate that the lowest-energy absorptions of both *closo*-compounds are attributable to the π - π^* transitions on the central terphenyl moieties, with minor contributions from the ICT transitions between the *o*-carborane and terphenyl groups as well. All calculated results based on the optimized S_0 structures are in good agreement with the experimentally observed UV/Vis absorption spectra.

In contrast, the calculated results for the S_1 states of *closo-DT* and *closo-PT* indicate that the major transitions associated with the low-energy emissions involve both HOMO \rightarrow LUMO and HOMO \rightarrow LUMO+1 transitions (Figure 3 and Table 2). Although the LUMO of each compound is significantly localized on the *o*-carborane moiety ($\sim 80\%$; Tables S2 and S4), each HOMO is predominantly located on the central terphenyl group ($>92\%$). These results strongly suggest that the experimentally observed emissions in the low-energy regions mainly originate from ICT transitions between the *o*-carborane and terphenyl moieties. In addition, each LUMO+1 is mainly located on the central terphenyl group ($>86\%$; Tables S2 and S4), strongly indicating that the intense emissions observed in the high-energy region, centered at ~ 350 nm for *closo-DT* and ~ 370 nm for *closo-PT*, originate from $\pi-\pi^*$ transitions in the terphenyl moieties, i.e., LE-based emissions. Consequently, the electronic transitions that occur in each *o*-carboranyl compound were precisely predicted using computational methods.

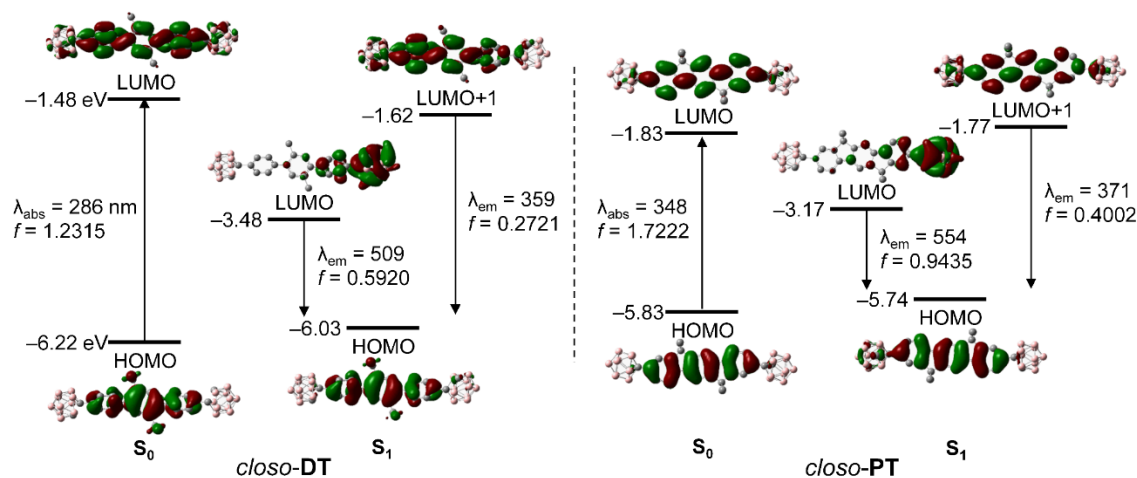


Figure 3. Frontier molecular orbitals of *closo-DT* and *closo-PT* in their ground states (S_0) and first excited singlet states (S_1), and their relative energies calculated by DFT (isovalue = 0.04). The transition energy (in nm) was calculated using the TD-B3LYP/6-31G(d) level of theory.

Table 2. Major low-energy electronic transitions in *closo-DT* and *closo-PT* involving their ground states (S_0) and first excited singlet states (S_1) calculated using the TD-B3LYP/6-31G(d) level of theory ¹.

	State	$\lambda_{\text{calc}}/\text{nm}$	f_{calc}	Assignment
<i>closo-DT</i>	S_0	285.7	1.2315	HOMO \rightarrow LUMO (98.0%)
	S_1	509.37	0.592	HOMO \rightarrow LUMO (99.6%)
<i>closo-PT</i>	S_0	348.17	1.7222	HOMO \rightarrow LUMO (98.8%)
	S_1	554.44	0.9435	HOMO \rightarrow LUMO (99.7%)
	S_1	371.34	0.4002	HOMO \rightarrow LUMO+1 (78.9%)

¹ Singlet energies for vertical transitions were calculated using optimized S_1 geometries.

2.4. Emission-Color Changes of Closo-*o*-Carboranyl Compounds Via Treatment of Fluoride Anion

Finally, to clarify the changes in the photoluminescence properties exhibited during the conversion of both *closo-DT* and *closo-PT* to the *nido*-species, we investigated the changes in the emissive patterns of both *closo*-compounds as a function of increasing amounts of TBAF in THF. These conversion processes of both *closo*-compounds to the respective *nido*-species by reaction with the fluoride anion occur consecutively, as clearly evidenced from the changes in the specific peaks of the $^1\text{H-NMR}$ spectra in THF- d_8 (Figure 4). The aryl protons of both *closo*-compounds in the region from 8.0 to 7.0 ppm shifted steadily to the upfield region upon increasing the concentration of TBAF, and finally, these peaks merged with the corresponding peaks in the spectra of each *nido*-compound in THF- d_8 , respectively. In particular, the broad singlet peaks around $\delta = -2.0$ and -2.5 ppm, which were assigned to the B-H-B

bridge protons of the *nido-o*-carborane, could be gradually monitored by increasing the concentration of TBAF. The results of $^1\text{H-NMR}$ spectral changes indicate that the conversion of the *closo*-compounds to the *nido*-species almost reached full conversion to that of corresponding pure *nido*-compounds when 5 equivalents of TBAF was used for the deboronation process.

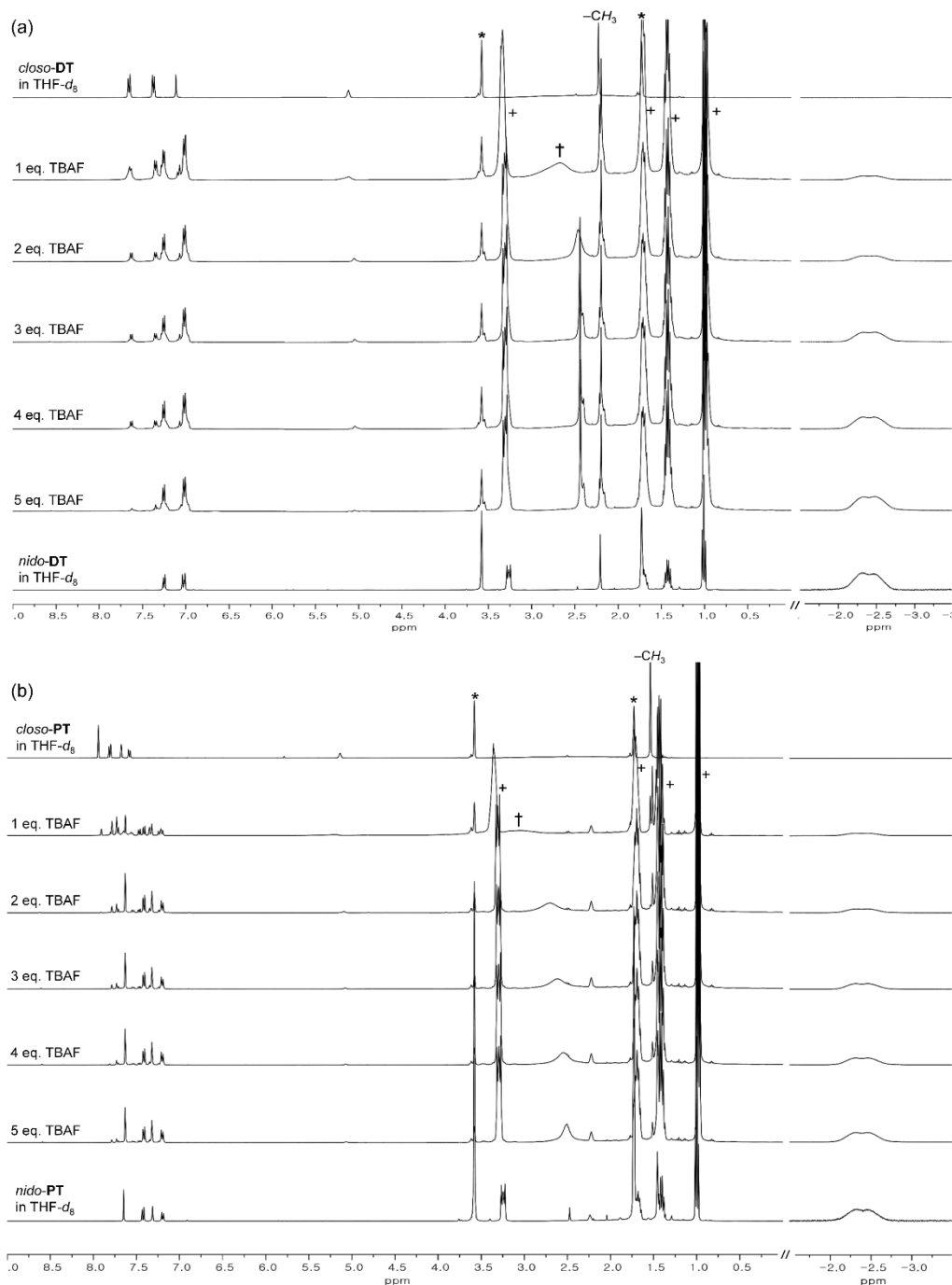


Figure 4. $^1\text{H-NMR}$ spectral changes of (a) *closo-DT* and (b) *closo-PT* upon increasing the amount of added fluoride anions and comparison with those of *nido-DT* and *nido-PT* (* from residual THF in $\text{THF-}d^8$, † from *n*-butyl group of excess TBAF, and + from *n*-butyl group for each *nido*-compound).

As illustrated in Figure 5, upon addition of incremental amounts of TBAF (0–5 equivalents) into the respective solutions of *closo-DT* and *closo-PT*, followed by heating at $60\text{ }^\circ\text{C}$ for 2 h, the LE-based emission for *closo-DT* ($\lambda_{\text{em}} = \sim 350\text{ nm}$) did not change significantly, whereas the ICT-based emission for

closo-PT ($\lambda_{em} = \sim 550$ nm) underwent gradual quenching, and eventually, a slightly enhanced LE-based emission ($\lambda_{em} \approx 380$ –410 nm) remained. In particular, the emission intensities and band shapes of each *closo*-compound after treatment with 5 equivalents of TBAF were mostly similar to those (Figure 5, red-solid lines) of the *nido*-compounds. Consequently, the conversion of *closo*-PT to *nido*-PT exhibited a vivid emission color change from orange to deep-blue (insets in Figure 5b), whereas *closo*-DT did not display any color changes from the emission in spite of the deboronation (insets in Figure 5a). These results demonstrate that degradation to the *nido*-form can not only prevent the ICT transition in the *o*-carboranyl compounds, but also reinforce the π - π^* -LE transition, which induces the emission color changes. Consequently, the luminescence-based color change response due to the alternation of the intrinsic electronic transitions caused by the reaction with fluoride anion and the structural feature of central terphenyl groups, indicates the potential of *closo*-PT as a naked-eye-detectable chemodosimeter for fluoride ion sensing.

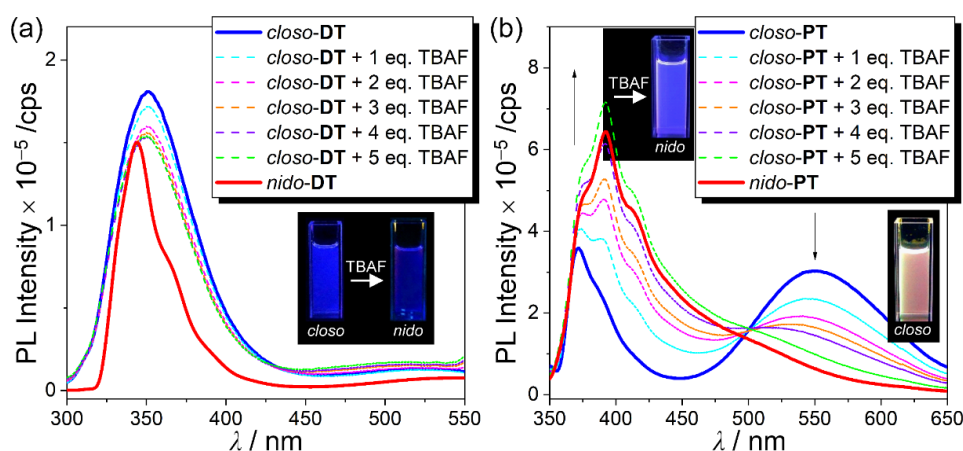


Figure 5. Spectral changes in the emission of (a) *closo*-DT (3.0×10^{-5} M, $\lambda_{ex} = 292$ nm) and (b) *closo*-PT (3.0×10^{-5} M, $\lambda_{ex} = 345$ nm) in THF in the presence of different amounts of TBAF, upon heating at 60 °C for 2 h. Insets are photographs of each *closo*- and *nido*-type (3.0×10^{-5} M in THF) under a UV lamp ($\lambda_{ex} = 295$ nm for DT derivatives and 365 nm for PT derivatives).

3. Materials and Methods

3.1. General Considerations

All operations were performed under an inert nitrogen atmosphere using standard Schlenk and glove-box techniques. Anhydrous solvents (toluene, trimethylamine (NEt₃), and methanol; Aldrich) were dried by passing through an activated alumina column and stored over activated molecular sieves (5 Å). Spectrophotometric-grade solvents (tetrahydrofuran (THF), toluene, dichloromethane (DCM), methanol, and *n*-hexane) were used as received from Alfa Aesar (Ward Hill, MA, USA). Commercial reagents were used without any further purification after purchase from Sigma-Aldrich (potassium carbonate (K₂CO₃), magnesium sulfate (MgSO₄) St. Louis, MO, USA), bis(triphenylphosphine)palladium(II) dichloride (Pd(PPh₃)₂Cl₂), copper(I) iodide (CuI), diethyl sulfide (Et₂S), ethynyltrimethylsilane, and poly(methyl methacrylate) (PMMA)). Decaborane (B₁₀H₁₄) was purchased from Alfa Aesar. The dibromo precursors, 4,4''-dibromo-2',5'-dimethyl-1,1':4',1''-terphenyl (DT1) and 2,8-dibromo-6,6,12,12-tetramethyl-6,12-dihydroindeno[1,2-*b*]fluorene (PT1), were prepared as reported in the literature [69]. CD₂Cl₂ and THF-*d*₈, purchased from Cambridge Isotope Laboratories, were dried over activated molecular sieves (5 Å). All nuclear magnetic resonance (NMR) spectra were recorded on a Bruker Avance 400 spectrometer (400.13 MHz for ¹H, 100.62 MHz for ¹³C, and 128.38 MHz for ¹¹B, Bruker, Billerica, MA, USA) at ambient temperature. Chemical shifts are given in ppm and are referenced against external Me₄Si (¹H and ¹³C) or BF₃·Et₂O (¹¹B). Elemental analysis was performed on an EA3000 instrument (Eurovector) at the Central Laboratory of Kangwon National University. UV–Vis absorption

and photoluminescence (PL) spectra were recorded on Jasco V-530 (Jasco, Easton, MD, USA) and Horiba FluoroMax-4P spectrophotometers (HORIBA, Edison, NJ, USA), respectively. Fluorescence decay lifetimes (τ_{obs}) were measured using a time-correlated single-photon counting spectrometer (FLS920, at the Central Laboratory of Kangwon National University, Edinburgh Instruments Ltd., Livingston, UK) equipped with an EPL 375 ps pulsed semiconductor diode laser as the excitation source and a microchannel plate photomultiplier tube (200–850 nm) as the detector, at 298 K. The absolute PL quantum yields (ϕ_{em}) were obtained with an absolute PL quantum yield spectrophotometer (HORIBA FluoroMax-4P equipped with an FM-SPHERE 3.2-inch internal integrating sphere, HORIBA, Edison, NJ, USA) at 298 K.

3.2. Synthesis of DT2

Triethylamine (16 mL) was added via cannulation to a mixture of DT1 (0.42 g, 1.0 mmol), copper iodide (15 mg), and Pd(PPh₃)₂Cl₂ (62 mg) at 25 °C. After stirring for 15 min, ethynyltrimethylsilane (0.55 mL, 4.0 mmol) was added, and the reaction mixture was heated at 90 °C with stirring for 24 h. After cooling to 25 °C, the volatiles were removed by rotary evaporation to afford a dark brown residue. The crude product was purified by column chromatography on silica gel (eluent: DCM/*n*-hexane = 1/10, *v/v*) to yield DT2 as a yellow solid, 0.28 g (yield = 62%). ¹H-NMR (CD₂Cl₂): δ 7.51 (d, *J* = 8.3 Hz, 4H), 7.32 (d, *J* = 8.4 Hz, 4H), 7.13 (s, 2H), 2.25 (s, 6H, –CH₃), 0.27 (s, 18H, –Si(CH₃)₃). ¹³C-NMR (CD₂Cl₂): δ 142.35, 140.71, 133.04, 132.05, 131.97, 129.60, 121.97, 105.26 (acetylene-C), 94.83 (acetylene-C), 20.01 (–CH₃), 0.03 (–Si(CH₃)₃). Anal. Calcd. for C₃₀H₃₄Si₂: C, 79.94; H, 7.60. Found: C, 79.87; H, 7.49.

3.3. Synthesis of PT2

PT2 was prepared according to a procedure analogous to that used for DT2, with PT1 (0.47 g, 1.0 mmol), copper iodide (15 mg), Pd(PPh₃)₂Cl₂ (62 mg), and ethynyltrimethylsilane (0.55 mL, 4.0 mmol), and was isolated as a yellow solid (0.42 g; yield = 83%). ¹H-NMR (CD₂Cl₂): δ 7.78 (s, 2H), 7.71 (d, *J* = 7.9 Hz, 2H), 7.55 (s, 2H), 7.45 (d, *J* = 7.8 Hz, 2H), 1.53 (s, 12H, –CH₃), 0.27 (s, 18H, –Si(CH₃)₃). ¹³C-NMR (CD₂Cl₂): δ 154.55, 154.16, 140.07, 138.92, 131.40, 126.63, 121.79, 120.08, 114.99, 106.24 (acetylene-C), 94.53 (acetylene-C), 46.96 (–C(CH₃)₂), 27.37 (–CH₃), 0.07 (–Si(CH₃)₃). Anal. Calcd. for C₃₄H₃₈Si₂: C, 81.21; H, 7.62. Found: C, 80.99; H, 7.55.

3.4. Synthesis of DT3

K₂CO₃ (0.28 g, 2.0 mmol) was dissolved in methanol (10 mL) and added to a solution of DT2 (0.23 g, 0.5 mmol) in DCM (5 mL). After stirring for 2 h at 25 °C, the resulting mixture was treated with DCM (50 mL) and the organic layer was separated. The aqueous layer was further extracted with DCM (20 × 2 mL). The combined organic extracts were dried over MgSO₄, filtered, and evaporated to dryness to afford a white residue. The crude product was purified by washing with *n*-hexane (10 mL) to yield DT3 as a white solid, 0.13 g (yield = 84%). ¹H-NMR (CD₂Cl₂): δ 7.56 (d, *J* = 8.0 Hz, 4H), 7.34 (d, *J* = 8.0 Hz, 4H), 7.13 (s, 2H), 3.18 (s, 2H, –CCH), 2.26 (s, 6H, –CH₃). ¹³C-NMR (CD₂Cl₂): δ 142.68, 140.68, 133.06, 132.24, 132.07, 129.66, 120.90, 83.81 (acetylene-C), 77.69 (acetylene-C), 20.01 (–CH₃). Anal. Calcd. for C₂₄H₁₈: C, 94.08; H, 5.92. Found: C, 93.77; H, 5.62.

3.5. Synthesis of PT3

PT3 was prepared according to a procedure analogous to that used for DT3 with PT2 (0.40 g, 0.8 mmol) and K₂CO₃ (0.44 g, 3.2 mmol), and was isolated as a white solid (0.25 g; yield = 88%). ¹H-NMR (CD₂Cl₂): δ 7.80 (s, 2H), 7.74 (d, *J* = 7.9 Hz, 2H), 7.59 (s, 2H), 7.50 (d, *J* = 7.8 Hz, 2H), 3.20 (s, 2H, –CCH), 1.54 (s, 12H, –CH₃). ¹³C-NMR (CD₂Cl₂): δ 154.59, 154.15, 140.34, 138.91, 131.64, 126.88, 120.72, 120.15, 115.06, 84.70 (acetylene-C), 77.44 (acetylene-C), 46.98 (–C(CH₃)₂), 27.36 (–CH₃). Anal. Calcd. for C₂₈H₂₂: C, 93.81; H, 6.19. Found: C, 93.77; H, 6.04.

3.6. Synthesis of *closo-DT*

Excess Et₂S (2.5 equiv., 1.2 mmol) was added at 25 °C to a solution of decaborane (B₁₀H₁₄, 0.52 mmol) and **DT3** (61 mg, 0.20 mmol) in toluene (20 mL). After heating to reflux, the reaction mixture was further stirred for 72 h. The solvent and volatiles were removed under vacuum and methanol (10 mL) was added. The resulting solid was filtered and redissolved in toluene. The crude product upon washing with *n*-hexane (15 mL), afforded *closo-DT* as a white solid (47 mg, Yield = 43%). ¹H{¹¹B} NMR (THF-*d*₈): δ 7.66 (d, *J* = 8.2 Hz, 4H), 7.38 (d, *J* = 8.1 Hz, 4H), 7.12 (s, 2H), 5.13 (s, 2H, CB-CH), 2.54 (br s, 8H, CB-BH), 2.39 (br s, 3H, CB-BH), 2.30 (br s, 9H, CB-BH), 2.23 (s, 6H, -CH₃). ¹³C-NMR (THF-*d*₈): δ 144.05, 140.59, 133.27, 133.24, 132.34, 130.14, 128.04, 77.58 (CB-C), 61.49 (CB-C), 19.74 (-CH₃). ¹¹B{¹H} NMR (THF-*d*₈): δ -4.44 (3B), -6.57 (1B), -10.84 (5B), -12.77 (7B), -14.67 (4B). Anal. Calcd. for C₂₈H₃₈B₂₀: C, 56.92; H, 6.48. Found: C, 56.79; H, 6.33.

3.7. Synthesis of *closo-PT*

Closo-PT was prepared according to a procedure analogous to that used for *closo-DT*, with decaborane (B₁₀H₁₄, 0.52 mmol), **PT3** (78 mg, 0.20 mmol), and Et₂S (2.5 equiv.). The crude product upon washing with *n*-hexane (15 mL), afforded *closo-PT* as a white solid (42 mg, Yield = 35%). ¹H{¹¹B} NMR (THF-*d*₈): δ 7.94 (s, 2H), 7.81 (d, *J* = 8.1 Hz, 2H), 7.67 (s, 2H), 7.58 (d, *J* = 7.9 Hz, 2H), 5.14 (s, 2H, CB-CH), 2.56 (br s, 7H, CB-BH), 2.50 (br s, 1H, CB-BH), 2.39 (br s, 2H, CB-BH), 2.30 (br s, 10H, CB-BH), 1.54 (s, 12H, -CH₃). ¹³C-NMR (THF-*d*₈): δ 155.41, 154.80, 141.67, 138.98, 133.36, 127.39, 122.52, 120.66, 115.65, 78.45 (CB-C), 61.55 (CB-C), 47.50 (-C(CH₃)₂), 27.08 (-CH₃). ¹¹B{¹H} NMR (THF-*d*₈): δ -2.73 (3B), -4.64 (1B), -9.09 (5B), -10.77 (7B), -12.86 (4B). Anal. Calcd. for C₃₂H₄₂B₂₀: C, 59.79; H, 6.59. Found: C, 59.87; H, 6.45.

3.8. Synthesis of *nido-DT*

Closo-DT (0.027 g, 0.05 mmol) was dissolved in 0.3 mL of a 0.2 M solution of *n*-tetrabutylammonium fluoride (TBAF) in THF at 25 °C. The reaction mixture was heated to reflux (60 °C) and stirred for 2 h. After cooling to 25 °C, the resulting mixture was treated with 50 mL of distilled water and 50 mL of DCM, and the organic portion was separated. The aqueous layer was further extracted with DCM (20 mL). The combined organic portions were dried over MgSO₄, filtered, and concentrated to dryness, affording a pale yellow residue. The crude product upon washing with methanol (15 mL), afforded *nido-DT* as a white solid (26 mg, Yield = 52%). ¹H{¹¹B} NMR: δ 7.28 (d, *J* = 8.0 Hz, 4H), 7.13 (d, *J* = 7.9 Hz, 4H), 7.07 (s, 2H), 3.11 (m, 16H, *n*-butyl-CH₂), 2.36 (s, 2H, CB-CH), 2.25 (s, 6H, -CH₃), 2.12 (br s, 4H, CB-BH), 1.88 (br s, 4H, CB-BH), 1.82 (br s, 4H, CB-BH), 1.62 (m, 16H, *n*-butyl-CH₂), 1.43 (m, 16H, *n*-butyl-CH₂), 1.26 (br s, 6H, CB-BH), 1.02 (t, *J* = 7.2 Hz, 24H, *n*-butyl-CH₃), -2.36 (br s, 2H, B-H-B). ¹³C NMR (CD₂Cl₂): δ 144.65, 140.78, 138.40, 132.83, 132.21, 128.64, 126.71, 59.43 (*n*-butyl-CH₂), 24.29 (*n*-butyl-CH₂), 20.18 (-CH₃), 20.10 (*n*-butyl-CH₂), 13.76 (*n*-butyl-CH₃). ¹¹B{¹H} NMR (CD₂Cl₂): δ -8.97 (3B), -10.43 (2B), -13.79 (1B), -18.28 (3B), -19.50 (1B), -23.00 (1B), -32.95 (3B), -36.10 (4B). Anal. Calcd. for C₆₀H₁₁₀B₁₈N₂: C, 68.37; H, 10.52; N, 2.66. Found: C, 68.11; H, 10.42; N, 2.54.

3.9. Synthesis of *nido-PT*

A procedure analogous to that for *nido-DT* was employed using *closo-PT* (0.027 g, 0.04 mmol) and 0.23 mL of a 0.2 M solution of TBAF in THF. The crude product, upon washing with methanol (15 mL), afforded *nido-PT* as a white solid (26 mg, Yield = 60%). ¹H{¹¹B} NMR (CD₂Cl₂): δ 7.65 (s, 2H), 7.49 (d, *J* = 7.9 Hz, 2H), 7.32 (s, 2H), 7.23 (d, *J* = 7.9 Hz, 2H), 3.08 (m, 16H, *n*-butyl-CH₂), 2.39 (s, 2H, CB-CH), 2.12 (br s, 4H, CB-BH), 2.00 (br s, 1H, CB-BH), 1.89 (br s, 5H, CB-BH), 1.60 (m, 16H, *n*-butyl-CH₂), 1.48 (s, 12H, -CH₃), 1.41 (m, 16H, *n*-butyl-CH₂), 1.31 (br s, 4H, CB-BH), 1.26 (br s, 4H, CB-BH), 1.00 (t, *J* = 7.2 Hz, 24H, *n*-butyl-CH₃), -2.34 (br s, 2H, B-H-B). ¹³C-NMR (CD₂Cl₂): δ 153.80, 153.54, 145.25, 138.62, 136.55, 126.10, 121.40, 118.72, 114.00, 59.40 (*n*-butyl-CH₂), 46.71 (-C(CH₃)₂), 27.74 (-CH₃), 24.27 (*n*-butyl-CH₂), 20.09 (*n*-butyl-CH₂), 13.75 (*n*-butyl-CH₃). ¹¹B{¹H} NMR (CD₂Cl₂): δ -8.91

(3B), −10.45 (2B), −13.68 (1B), −18.46 (3B), −19.47 (1B), −23.09 (1B), −32.95 (3B), −36.05 (4B). Anal. Calcd. for C₆₄H₁₁₄B₁₈N₂: C, 69.49; H, 10.39; N, 2.53. Found: C, 69.30; H, 10.16; N, 2.39.

3.10. UV/Vis Absorption and Photoluminescence (PL) Experiments

The solution-phase UV–Vis absorption and PL measurements of the *closo*- and *nido*-*o*-carboranyl compounds were performed in degassed organic solvents with a 1 cm quartz cuvette (3.0×10^{-5} M) at 298 K. PL measurements for the *closo*-compounds were also performed in THF at 77 K and in the film state (5 wt% doped in PMMA) on 1.5×1.5 cm quartz plates (thickness = 1 mm) at 298 K.

3.11. Computational Studies

The optimized geometries for the ground (S_0) and first excited (S_1) states of both *closo*-*o*-carboranyl compounds (*closo*-DT and *closo*-PT) in THF were obtained using the B3LYP/6-31G(d,p) [85] level of theory. The vertical excitation energies at the optimized S_0 geometries as well as the optimized geometries of the S_1 states were calculated using time-dependent density functional theory (TD-DFT) [86] at the same level of theory. Solvent effects were included using the conductor-like polarizable continuum model (CPCM) [83,84]. All geometry optimizations were performed using the Gaussian 16 program [87]. The percent contribution of a group in a molecule to each molecular orbital was calculated with the GaussSum 3.0 program [88]. Visualizations were prepared using GaussView 6 [89].

4. Conclusions

We herein reported the preparation and characterization of distorted and planar terphenyl-based *closo*- (*closo*-DT and *closo*-PT) and *nido*- (*nido*-DT and *nido*-PT) *o*-carboranyl compounds. Although *closo*-DT exhibited strong π – π^* LE-based emission in THF at 298 K in the high-energy region, *closo*-PT demonstrated intense emission in the low-energy region that was attributable to the ICT transitions involving the *o*-carborane cage. Interestingly, both *nido*-compounds exhibited LE-based emission alone in the same condition due to the anionic character of the *nido*-*o*-carborane cages, which cannot cause the ICT transitions. Consequently, the successful deboronation of *closo*-PT to *nido*-PT upon exposure to increasing concentration of fluoride anion leads to ratiometric emission color change from orange to deep-blue in solution. Such results strongly imply that the fine-tuning of electronic and structural features, which can control the ICT-based emission, shows the potential of *closo*-*o*-carboranyl compounds as candidates for naked-eye-detectable chemodosimeters for fluoride ion-sensing.

Supplementary Materials: The following are available online. Multinuclear NMR spectra (¹H, ¹³C, and ¹¹B) of the *closo*- and *nido*-*o*-carboranyl compounds and their precursors (Figures S1–S12), and photophysical (Figures S13–S14) and computational data (Figures S15–S16 and Tables S1–S8).

Author Contributions: H.S., M.S.M., M.K., and J.H.K. synthesized the compounds and analyzed the data. D.K.A. and K.M.L. analyzed the data and wrote the paper. J.H.L. and H.H. conducted the computational study, analyzed the data, and wrote the paper. All authors have read and agreed to the published version of the manuscript.

Funding: This research was funded by the National Research Foundation of Korea (NRF) grant (NRF-2016M3A7B4909246, NRF-2017R1D1A1B03035412, NRF-2018R1D1A1B07040387, and NRF-2020R1A2C1006400) funded by the Ministry of Science and ICT and the Ministry of Education.

Acknowledgments: We thank Seonah Kim and Chan Hee Ryu (Department of Chemistry, Institute for Molecular Science and Fusion Technology, Kangwon National University) for assistance with design of synthetic routes for *o*-carboranyl compounds.

Conflicts of Interest: The authors declare no conflicts of interest.

References

1. Bregadze, V.I. Dicarba-closo-dodecaboranes $C_2B_{10}H_{12}$ and their derivatives. *Chem. Rev.* **1992**, *92*, 209–223. [[CrossRef](#)]
2. González-Campo, A.; Juárez-Pérez, E.J.; Viñas, C.; Boury, B.; Sillanpää, R.; Kivekäs, R.; Núñez, R. Carboranyl Substituted Siloxanes and Octasilsesquioxanes: Synthesis, Characterization, and Reactivity. *Macromolecules* **2008**, *41*, 8458–8466. [[CrossRef](#)]
3. Issa, F.; Kassiou, M.; Rendina, L.M. Boron in Drug Discovery: Carboranes as Unique Pharmacophores in Biologically Active Compounds. *Chem. Rev.* **2011**, *111*, 5701–5722. [[CrossRef](#)]
4. Wee, K.-R.; Cho, Y.-J.; Jeong, S.; Kwon, S.; Lee, J.-D.; Suh, I.-H.; Kang, S.O. Carborane-Based Optoelectronically Active Organic Molecules: Wide Band Gap Host Materials for Blue Phosphorescence. *J. Am. Chem. Soc.* **2012**, *134*, 17982–17990. [[CrossRef](#)] [[PubMed](#)]
5. Ferrer-Ugalde, A.; Juárez-Pérez, E.J.; Teixidor, F.; Viñas, C.; Núñez, R. Synthesis, Characterization, and Thermal Behavior of Carboranyl–Styrene Decorated Octasilsesquioxanes: Influence of the Carborane Clusters on Photoluminescence. *Chem. Eur. J.* **2013**, *19*, 17021–17030. [[CrossRef](#)] [[PubMed](#)]
6. Kim, T.; Kim, H.; Lee, K.M.; Lee, Y.S.; Lee, M.H. Phosphorescence Color Tuning of Cyclometalated Iridium Complexes by *o*-Carborane Substitution. *Inorg. Chem.* **2013**, *52*, 160–168. [[CrossRef](#)]
7. Bae, H.J.; Chung, J.; Kim, H.; Park, J.; Lee, K.M.; Koh, T.-W.; Lee, Y.S.; Yoo, S.; Do, Y.; Lee, M.H. Deep Red Phosphorescence of Cyclometalated Iridium Complexes by *o*-Carborane Substitution. *Inorg. Chem.* **2014**, *53*, 128–138. [[CrossRef](#)]
8. Asay, M.J.; Fisher, S.P.; Lee, S.E.; Tham, F.S.; Borchardt, D.; Lavallo, V. Synthesis of unsymmetrical *N*-carboranyl NHCs: Directing effect of the carborane anion. *Chem. Commun.* **2015**, *51*, 5359–5362. [[CrossRef](#)]
9. Lee, Y.H.; Park, J.; Jo, S.-J.; Kim, M.; Lee, J.; Lee, S.U.; Lee, M.H. Manipulation of Phosphorescence Efficiency of Cyclometalated Iridium Complexes by Substituted *o*-Carboranes. *Chem. Eur. J.* **2015**, *21*, 2052–2061. [[CrossRef](#)]
10. Núñez, R.; Tarrés, M.; Ferrer-Ugalde, A.; Fabrizi de Biani, F.; Teixidor, F. Electrochemistry and Photoluminescence of Icosahedral Carboranes, Boranes, Metallocarboranes, and Their Derivatives. *Chem. Rev.* **2016**, *116*, 14307–14378. [[CrossRef](#)]
11. Mukherjee, S.; Thilagar, P. Boron clusters in luminescent materials. *Chem. Commun.* **2016**, *52*, 1070–1093. [[CrossRef](#)]
12. Dziedzic, R.M.; Saleh, L.M.A.; Axtell, J.C.; Martin, J.L.; Stevens, S.L.; Royappa, A.T.; Rheingold, A.L.; Spokoyny, A.M. B–N, B–O, and B–CN Bond Formation via Palladium-Catalyzed Cross-Coupling of B-Bromo-Carboranes. *J. Am. Chem. Soc.* **2016**, *138*, 9081–9084. [[CrossRef](#)]
13. Kirlikovali, K.O.; Axtell, J.C.; Gonzalez, A.; Phung, A.C.; Khan, S.I.; Spokoyny, A.M. Luminescent metal complexes featuring photophysically innocent boron cluster ligands. *Chem. Sci.* **2016**, *7*, 5132–5138. [[CrossRef](#)]
14. Saleh, L.M.A.; Dziedzic, R.M.; Khan, S.I.; Spokoyny, A.M. Forging Unsupported Metal–Boryl Bonds with Icosahedral Carboranes. *Chem. Eur. J.* **2016**, *22*, 8466–8470. [[CrossRef](#)]
15. Eleazer, B.J.; Smith, M.D.; Popov, A.A.; Peryshkov, D.V. (BB)-Carboryne Complex of Ruthenium: Synthesis by Double B–H Activation at a Single Metal Center. *J. Am. Chem. Soc.* **2016**, *138*, 10531–10538. [[CrossRef](#)]
16. Wong, Y.O.; Smith, M.D.; Peryshkov, D.V. Synthesis of the First Example of the 12-Vertex-closo/12-Vertex-nido Biscarborane Cluster by a Metal-Free B–H Activation at a Phosphorus(III) Center. *Chem. Eur. J.* **2016**, *22*, 6764–6767. [[CrossRef](#)] [[PubMed](#)]
17. Chan, A.L.; Estrada, J.; Kefalidis, C.E.; Lavallo, V. Changing the Charge: Electrostatic Effects in Pd-Catalyzed Cross-Coupling. *Organometallics* **2016**, *35*, 3257–3260. [[CrossRef](#)]
18. Fisher, S.P.; El-Hellani, A.; Tham, F.S.; Lavallo, V. Anionic and zwitterionic carboranyl *N*-heterocyclic carbene Au(I) complexes. *Dalton Trans.* **2016**, *45*, 9762–9765. [[CrossRef](#)] [[PubMed](#)]
19. Kim, Y.; Park, S.; Lee, Y.H.; Jung, J.; Yoo, S.; Lee, M.H. Homoleptic Tris-Cyclometalated Iridium Complexes with Substituted *o*-Carboranes: Green Phosphorescent Emitters for Highly Efficient Solution-Processed Organic Light-Emitting Diodes. *Inorg. Chem.* **2016**, *55*, 909–917. [[CrossRef](#)]
20. Tu, D.; Leong, P.; Guo, S.; Yan, H.; Lu, C.; Zhao, Q. Highly Emissive Organic Single-Molecule White Emitters by Engineering *o*-Carborane-Based Luminophores. *Angew. Chem. Int. Ed.* **2017**, *56*, 11370–11374. [[CrossRef](#)]

21. Kirlikovali, K.O.; Axtell, J.C.; Anderson, K.; Djurovich, P.I.; Rheingold, A.L.; Spokoyny, A.M. Fine-Tuning Electronic Properties of Luminescent Pt(II) Complexes via Vertex-Differentiated Coordination of Sterically Invariant Carborane-Based Ligands. *Organometallics* **2018**, *37*, 3122–3131. [[CrossRef](#)]
22. Nar, I.; Atsay, A.; Altındal, A.; Hamuryudan, E. *o*-Carborane, Ferrocene, and Phthalocyanine Triad for High-Mobility Organic Field-Effect Transistors. *Inorg. Chem.* **2018**, *57*, 2199–2208. [[CrossRef](#)] [[PubMed](#)]
23. Grimes, R.N. *Carboranes*, 2nd ed.; Academic Press: London, UK, 2011.
24. Spokoyny, A.M. New ligand platforms featuring boron-rich clusters as organomimetic substituents. *Pure Appl. Chem.* **2013**, *85*, 903–919. [[CrossRef](#)]
25. Poater, J.; Solà, M.; Viñas, C.; Teixidor, F. π Aromaticity and Three-Dimensional Aromaticity: Two sides of the Same Coin? *Angew. Chem. Int. Ed.* **2014**, *53*, 12191–12195. [[CrossRef](#)]
26. Poater, J.; Solà, M.; Viñas, C.; Teixidor, F. Hückel's Rule of Aromaticity Categorizes Aromatic *closo* Boron Hydride Clusters. *Chem. Eur. J.* **2016**, *22*, 7437–7443. [[CrossRef](#)] [[PubMed](#)]
27. Núñez, R.; Romero, I.; Teixidor, F.; Viñas, C. Icosahedral boron clusters: A perfect tool for the enhancement of polymer features. *Chem. Soc. Rev.* **2016**, *45*, 5147–5173. [[CrossRef](#)]
28. Cabrera-González, J.; Sánchez-Arderiu, V.; Viñas, C.; Parella, T.; Teixidor, F.; Núñez, R. Redox-Active Metallocarborane-Decorated Octasilsesquioxanes. Electrochemical and Thermal Properties. *Inorg. Chem.* **2016**, *55*, 11630–11634. [[CrossRef](#)]
29. Kokado, K.; Chujo, Y. Multicolor Tuning of Aggregation-Induced Emission through Substituent Variation of Diphenyl-*o*-carborane. *J. Org. Chem.* **2011**, *76*, 316–319. [[CrossRef](#)]
30. Dash, B.P.; Satapathy, R.; Gaillard, E.R.; Norton, K.M.; Maguire, J.A.; Chug, N.; Hosmane, N.S. Enhanced π -Conjugation and Emission via Icosahedral Carboranes: Synthetic and Spectroscopic Investigation. *Inorg. Chem.* **2011**, *50*, 5485–5493. [[CrossRef](#)]
31. Wee, K.-R.; Han, W.-S.; Cho, D.W.; Kwon, S.; Pac, C.; Kang, S.O. Carborane photochemistry triggered by aryl substitution: Carborane-based dyads with phenyl carbazoles. *Angew. Chem. Int. Ed.* **2012**, *51*, 2677–2680. [[CrossRef](#)]
32. Weber, L.; Kahlert, J.; Brockhinke, R.; Böhling, L.; Brockhinke, A.; Stammer, H.-G.; Neumann, B.; Harder, R.A.; Fox, M.A. Luminescence Properties of *C*-Diazaborolyl-*ortho*-Carboranes as Donor–Acceptor Systems. *Chem. Eur. J.* **2012**, *18*, 8347–8357. [[CrossRef](#)] [[PubMed](#)]
33. Bae, H.J.; Kim, H.; Lee, K.M.; Kim, T.; Eo, M.; Lee, Y.S.; Do, Y.; Lee, M.H. Heteroleptic tris-cyclometalated iridium(III) complexes supported by an *o*-carboranyl-pyridine ligand. *Dalton Trans.* **2013**, *42*, 8549–8552. [[CrossRef](#)] [[PubMed](#)]
34. Weber, L.; Kahlert, J.; Brockhinke, R.; Böhling, L.; Halama, J.; Brockhinke, A.; Stammer, H.-G.; Neumann, B.; Nervi, C.; Harder, R.A.; et al. *C,C'*-Bis(benzodiazaborolyl)dicarba-*closo*-dodecaboranes: Synthesis, structures, photophysics and electrochemistry. *Dalton Trans.* **2013**, *42*, 10982–10996. [[CrossRef](#)] [[PubMed](#)]
35. Weber, L.; Kahlert, J.; Böhling, L.; Brockhinke, A.; Stammer, H.-G.; Neumann, B.; Harder, R.A.; Low, P.J.; Fox, M.A. Electrochemical and spectroelectrochemical studies of *C*-benzodiazaborolyl-*ortho*-carboranes. *Dalton Trans.* **2013**, *42*, 2266–2281. [[CrossRef](#)] [[PubMed](#)]
36. Kwon, S.; Wee, K.-R.; Cho, Y.-J.; Kang, S.O. Carborane Dyads for Photoinduced Electron Transfer: Photophysical Studies on Carbazole and Phenyl-*o*-carborane Molecular Assemblies. *Chem. Eur. J.* **2014**, *20*, 5953–5960. [[CrossRef](#)]
37. Ferrer-Ugalde, A.; González-Campo, A.; Viñas, C.; Rodríguez-Romero, J.; Santillan, R.; Farfán, N.; Sillanpää, R.; Sousa-Pedrares, A.; Núñez, R.; Teixidor, F. Fluorescence of New *o*-Carborane Compounds with Different Fluorophores: Can it be Tuned? *Chem. Eur. J.* **2014**, *20*, 9940–9951. [[CrossRef](#)]
38. Bae, H.J.; Kim, H.; Lee, K.M.; Kim, T.; Lee, Y.S.; Do, Y.; Lee, M.H. Through-space charge transfer and emission color tuning of di-*o*-carborane substituted benzene. *Dalton Trans.* **2014**, *43*, 4978–4985. [[CrossRef](#)]
39. Lee, Y.H.; Park, J.; Lee, J.; Lee, S.U.; Lee, M.H. Iridium Cyclometalates with Tethered *o*-Carboranes: Impact of Restricted Rotation of *o*-Carborane on Phosphorescence Efficiency. *J. Am. Chem. Soc.* **2015**, *137*, 8018–8021. [[CrossRef](#)]
40. Naito, H.; Morisaki, Y.; Chujo, Y. *o*-Carborane-Based Anthracene: A Variety of Emission Behaviors. *Angew. Chem. Int. Ed.* **2015**, *54*, 5084–5087. [[CrossRef](#)]
41. Kim, T.; Lee, J.; Lee, S.U.; Lee, M.H. *o*-Carboranyl–Phosphine as a New Class of Strong-Field Ancillary Ligand in Cyclometalated Iridium(III) Complexes: Toward Blue Phosphorescence. *Organometallics* **2015**, *34*, 3455–3458. [[CrossRef](#)]

42. Choi, B.H.; Lee, J.H.; Hwang, H.; Lee, K.M.; Park, M.H. Novel Dimeric *o*-Carboranyl Triarylborane: Intriguing Ratiometric Color-Tunable Sensor via Aggregation-Induced Emission by Fluoride Anions. *Organometallics* **2016**, *35*, 1771–1777. [[CrossRef](#)]
43. Wee, K.-R.; Cho, Y.-J.; Song, J.K.; Kang, S.O. Multiple photoluminescence from 1,2-dinaphthyl-ortho-carborane. *Angew. Chem. Int. Ed.* **2013**, *52*, 9682–9685. [[CrossRef](#)] [[PubMed](#)]
44. Naito, H.; Nishino, K.; Morisaki, Y.; Tanaka, K.; Chujo, Y. Solid-State Emission of the Anthracene-*o*-Carborane Dyad from the Twisted-Intramolecular Charge Transfer in the Crystalline State. *Angew. Chem. Int. Ed.* **2017**, *56*, 254–259. [[CrossRef](#)] [[PubMed](#)]
45. Wu, X.; Guo, J.; Cao, Y.; Zhao, J.; Jia, W.; Chen, Y.; Jia, D. Mechanically triggered reversible stepwise tricolor switching and thermochromism of anthracene-*o*-carborane dyad. *Chem. Sci.* **2018**, *9*, 5270–5277. [[CrossRef](#)] [[PubMed](#)]
46. Li, J.; Yang, C.; Peng, X.; Chen, Y.; Qi, Q.; Luo, X.; Lai, W.-Y.; Huang, W. Stimuli-responsive solid-state emission from *o*-carborane–tetraphenylethene dyads induced by twisted intramolecular charge transfer in the crystalline state. *J. Mater. Chem. C.* **2018**, *6*, 19–28. [[CrossRef](#)]
47. Nishino, K.; Yamamoto, H.; Tanaka, K.; Chujo, Y. Development of Solid-State Emissive Materials Based on Multifunctional *o*-Carborane–Pyrene Dyads. *Org. Lett.* **2016**, *18*, 4064–4067. [[CrossRef](#)] [[PubMed](#)]
48. Wu, X.; Guo, J.; Zhao, J.; Che, Y.; Jia, D.; Chen, Y. Multifunctional luminescent molecules of *o*-carborane-pyrene dyad/triad: Flexible synthesis and study of the photophysical properties. *Dyes and Pigm.* **2018**, *154*, 44–51. [[CrossRef](#)]
49. Marsh, A.V.; Cheetham, N.J.; Little, M.; Dyson, M.; White, A.J.P.; Beavis, P.; Warriner, C.N.; Swain, A.C.; Stavrinou, P.N.; Heeney, M. Carborane-Induced Excimer Emission of Severely Twisted Bis-*o*-Carboranyl Chrysene. *Angew. Chem. Int. Ed.* **2018**, *57*, 10640–10645. [[CrossRef](#)]
50. Kim, S.-Y.; Cho, Y.-J.; Jin, G.F.; Han, W.-S.; Son, H.-J.; Cho, D.W.; Kang, S.O. Intriguing emission properties of triphenylamine–carborane systems. *Phys. Chem. Chem. Phys.* **2015**, *17*, 15679–15682. [[CrossRef](#)]
51. Wan, Y.; Li, J.; Peng, X.; Huang, C.; Qi, Q.; Lai, W.-Y.; Huang, W. Intramolecular charge transfer induced emission from triphenylamine-*o*-carborane dyads. *RSC Adv.* **2017**, *7*, 35543–35548. [[CrossRef](#)]
52. Nishino, K.; Uemura, K.; Gon, M.; Tanaka, K.; Chujo, Y. Enhancement of Aggregation-Induced Emission by Introducing Multiple *o*-Carborane Substitutions into Triphenylamine. *Molecules.* **2017**, *22*, 2009. [[CrossRef](#)] [[PubMed](#)]
53. Nishino, K.; Uemura, K.; Tanaka, K.; Morisaki, Y.; Chujo, Y. Modulation of the *cis*- and *trans*-Conformations in Bis-*o*-carborane Substituted Benzodithiophenes and Emission Enhancement Effect on Luminescent Efficiency by Solidification. *Eur. J. Org. Chem.* **2018**, *12*, 1507–1512. [[CrossRef](#)]
54. Ferrer-Ugalde, A.; Juárez-Pérez, E.J.; Teixidor, F.; Viñas, C.; Sillanpää, R.; Pérez-Inestrosa, E.; Núñez, R. Synthesis and Characterization of New Fluorescent Styrene-Containing Carborane Derivatives: The Singular Quenching Role of a Phenyl Substituent. *Chem. Eur. J.* **2012**, *18*, 544–553. [[CrossRef](#)] [[PubMed](#)]
55. Tu, D.; Leong, P.; Li, Z.; Hu, R.; Shi, C.; Zhang, K.Y.; Yan, H.; Zhao, Q. A carborane-triggered metastable charge transfer state leading to spontaneous recovery of mechanochromic luminescence. *Chem. Commun.* **2016**, *52*, 12494–12497. [[CrossRef](#)] [[PubMed](#)]
56. Ferrer-Ugalde, A.; Cabrera-González, J.; Juárez-Pérez, E.J.; Teixidor, F.; Pérez-Inestrosa, E.; Montenegro, J.M.; Sillanpää, R.; Haukka, M.; Núñez, R. Carborane–stilbene dyads: The influence of substituents and cluster isomers on photoluminescence properties. *Dalton Trans.* **2017**, *46*, 2091–2104. [[CrossRef](#)]
57. Li, X.; Yin, Y.; Yan, H.; Lu, C. Aggregation-Induced Emission Characteristics of *o*-Carborane-Functionalized Tetraphenylethylene Luminogens: The Influence of Carborane Cages on Photoluminescence. *Chem. Asian J.* **2017**, *12*, 2207–2210. [[CrossRef](#)]
58. Kaiser, R.P.; Mosinger, J.; Císařová, I.; Kotora, M. Synthesis of selectively 4-substituted 9,9'-spirobifluorenes and modulation of their photophysical properties. *Org. Biomol. Chem.* **2017**, *15*, 6913–6920. [[CrossRef](#)]
59. Santos, W.G.; Budkina, D.S.; Deflon, V.M.; Tarnovsky, A.N.; Cardoso, D.R.; Forbes, M.D.E. Photoinduced Charge Shifts and Electron Transfer in Viologen–Tetraphenylborate Complexes: Push–Pull Character of the Exciplex. *J. Am. Chem. Soc.* **2017**, *139*, 7681–7684. [[CrossRef](#)]
60. Naito, H.; Nishino, K.; Morisaki, Y.; Tanaka, K.; Chujo, Y. Luminescence Color Tuning from Blue to Near Infrared of Stable Luminescent Solid Materials Based on Bis-*o*-Carborane-Substituted Oligoacenes. *Chem. Asian J.* **2017**, *12*, 2134–2138. [[CrossRef](#)]

61. Naito, H.; Nishino, K.; Morisaki, Y.; Tanaka, K.; Chujo, Y. Highly-efficient solid-state emissions of anthracene-*o*-carborane dyads with various substituents and their thermochromic luminescence properties. *J. Mater. Chem. C* **2017**, *5*, 10047–10054. [[CrossRef](#)]
62. Wu, X.; Guo, J.; Quan, Y.; Jia, W.; Jia, D.; Chen, Y.; Xie, Z. Cage carbon-substitute does matter for aggregation-induced emission features of *o*-carborane-functionalized anthracene triads. *J. Mater. Chem. C* **2018**, *6*, 4140–4149. [[CrossRef](#)]
63. Mori, H.; Nishino, K.; Wada, K.; Morisaki, Y.; Tanaka, K.; Chujo, Y. Modulation of luminescence chromic behaviors and environment-responsive intensity changes by substituents in bis-*o*-carborane-substituted conjugated molecules. *Mater. Chem. Front.* **2018**, *2*, 573–579. [[CrossRef](#)]
64. Chen, Y.; Guo, J.; Wu, X.; Jia, D.; Tong, F. Color-tuning aggregation-induced emission of *o*-Carborane-bis(1,3,5-triaryl-2-pyrazoline) triads: Preparation and investigation of the photophysics. *Dyes Pigm.* **2018**, *148*, 180–188. [[CrossRef](#)]
65. Kim, S.-Y.; Lee, J.-D.; Cho, Y.-J.; Son, M.R.; Son, H.-J.; Cho, D.W.; Kang, S.O. Excitation spectroscopic and synchronous fluorescence spectroscopic analysis of the origin of aggregation-induced emission in *N,N*-diphenyl-1-naphthylamine-*o*-carborane derivatives. *Phys. Chem. Chem. Phys.* **2018**, *20*, 17458–17463. [[CrossRef](#)] [[PubMed](#)]
66. Shin, N.; Yu, S.; Lee, J.H.; Hwang, H.; Lee, K.M. Biphenyl- and Fluorene-Based *o*-Carboranyl Compounds: Alteration of Photophysical Properties by Distortion of Biphenyl Rings. *Organometallics* **2017**, *36*, 1522–1529. [[CrossRef](#)]
67. Jin, H.; Bae, H.J.; Kim, S.; Lee, J.H.; Hwang, H.; Park, M.H.; Lee, K.M. 2-Phenylpyridine- and 2-(benzo[*b*]thiophen-2-yl)pyridine-based *o*-carboranyl compounds: Impact of the structural formation of aromatic rings on photophysical properties. *Dalton Trans.* **2019**, *48*, 1467–1476. [[CrossRef](#)]
68. Jin, H.; Kim, S.; Bae, H.J.; Lee, J.H.; Hwang, H.; Park, M.H.; Lee, K.M. Effect of Planarity of Aromatic Rings Appended to *o*-Carborane on Photophysical Properties: A Series of *o*-Carboranyl Compounds Based on 2-Phenylpyridine- and 2-(Benzo[*b*]thiophen-2-yl)pyridine. *Molecules* **2019**, *24*, 201. [[CrossRef](#)]
69. So, H.; Kim, J.H.; Lee, J.H.; Hwang, H.; An, D.K.; Lee, K.M. Planarity of terphenyl rings possessing *o*-carborane cages: Turning on intramolecular-charge-transfer-based emission. *Chem. Commun.* **2019**, *55*, 14518. [[CrossRef](#)]
70. Kim, S.; Lee, J.H.; So, H.; Ryu, J.; Lee, J.; Hwang, H.; Kim, Y.; Park, M.H.; Lee, K.M. Spirobifluorene-Based *o*-Carboranyl Compounds: Insights into the Rotational Effect of Carborane Cages on Photoluminescence. *Chem. Eur. J.* **2020**, *26*, 548. [[CrossRef](#)]
71. Nishino, K.; Morisaki, Y.; Tanaka, K.; Chujo, Y. Electron-donating abilities and luminescence properties of tolane-substituted *nido*-carboranes. *New J. Chem.* **2017**, *41*, 10550. [[CrossRef](#)]
72. Fox, M.A.; Gill, W.R.; Herbertson, P.L.; MacBride, J.A.H.; Wade, K.; Colquhoun, H.M. Deboronation of C-substituted *ortho*- and *meta-closo*-carboranes using “wet” fluoride ion solutions. *Polyhedron* **1996**, *15*, 565. [[CrossRef](#)]
73. Yoo, J.; Hwang, J.-W.; Do, Y. Facile and Mild Deboronation of *o*-Carboranes Using Cesium Fluoride. *Inorg. Chem.* **2001**, *40*, 568. [[CrossRef](#)]
74. Peterson, J.J.; Werre, M.; Simon, Y.C.; Coughlin, E.B.; Carter, K.R. Carborane-Containing Polyfluorene: *O*-Carborane in the Main Chain. *Macromolecules* **2009**, *42*, 8594. [[CrossRef](#)]
75. Lerouge, F.; Ferrer-Ugalde, A.; Viñas, C.; Teixidor, F.; Sillanpää, R.; Abreu, A.; Xochitiotzi, E.; Farfán, N.; Santillan, R.; Núñez, R. Synthesis and fluorescence emission of neutral and anionic di- and tetra-carboranyl compounds. *Dalton Trans.* **2011**, *40*, 7541. [[CrossRef](#)]
76. Park, M.H.; Lee, K.M.; Kim, T.; Do, Y.; Lee, M.H. *Ortho*-Carborane-Functionalized Luminescent Polyethylene: Potential Chemodosimeter for the Sensing of Nucleophilic Anions. *Chem. Asian J.* **2011**, *6*, 1362. [[CrossRef](#)]
77. You, D.K.; Lee, J.H.; Hwang, H.; Kwon, H.; Park, M.H.; Lee, K.M. Deboronation-induced ratiometric emission sensing of fluoride by 1,3,5-tris(*o*-carboranyl-methyl)benzene. *Tetrahedron Lett.* **2017**, *58*, 3246. [[CrossRef](#)]
78. Song, K.C.; Kim, H.; Lee, K.M.; Lee, Y.S.; Do, Y.; Lee, M.H. Dual sensing of fluoride ions by the *o*-carborane-triarylborane dyad. *Dalton Trans.* **2013**, *42*, 2351. [[CrossRef](#)]
79. Hawthorne, M.F.; Berry, T.E.; Wegner, P.A. The Electronic Properties of the 1,2- and 1,7-Dicarbaclvododecaborane(12) Groups Bonded at Carbon. *J. Am. Chem. Soc.* **1965**, *87*, 4746–4750. [[CrossRef](#)]

80. Paxson, T.E.; Callahan, K.P.; Hawthorne, M.F. Improved synthesis of biscarborane and its precursor ethynylcarborane. *Inorg. Chem.* **1973**, *12*, 708–709. [[CrossRef](#)]
81. Jiang, W.; Knobler, C.B.; Hawthorne, M.F. Synthesis and Structural Characterization of Bis- and Tris(*closo*-1,2-C₂B₁₀H₁₁-1-yl)-Substituted Biphenyl and Benzene. *Inorg. Chem.* **1996**, *35*, 3056–3058. [[CrossRef](#)]
82. Lee, J.H.; Hwang, H.; Lee, K.M. *p*-Terphenyl-based di-*o*-carboranyl compounds: Alteration of electronic transition state by terminal phenyl groups. *J. Organomet. Chem.* **2016**, *825–826*, 69–74. [[CrossRef](#)]
83. Cossi, M.; Rega, N.; Scalmani, G.; Barone, V. Energies, structures, and electronic properties of molecules in solution with the C-PCM solvation model. *J. Comput. Chem.* **2003**, *24*, 669–681. [[CrossRef](#)] [[PubMed](#)]
84. Barone, V.; Cossi, M. Quantum Calculation of Molecular Energies and Energy Gradients in Solution by a Conductor Solvent Model. *J. Phys. Chem. A.* **1998**, *102*, 1995–2001. [[CrossRef](#)]
85. Binkley, J.S.; Pople, J.A.; Hehre, W.J. Self-consistent molecular orbital methods. 21. Small split-valence basis sets for first-row elements. *J. Am. Chem. Soc.* **1980**, *102*, 939–947. [[CrossRef](#)]
86. Runge, E.; Gross, E.K.U. Density-Functional Theory for Time-Dependent Systems. *Phys. Rev. Lett.* **1984**, *52*, 997. [[CrossRef](#)]
87. *Gaussian*, version 09 B.01; Gaussian, Inc.: Wallingford, CT, USA, 2016.
88. O'Boyle, N.M.; Tenderholt, A.L.; Langner, K.M. cclib: A library for package-independent computational chemistry algorithms. *J. Comp. Chem.* **2008**, *29*, 839–845. [[CrossRef](#)]
89. *GaussView*, version 6; Semichem Inc.: Shawnee Mission, KS, USA, 2016.

Sample Availability: Samples of the *o*-carboranyl compounds are available from the authors.



© 2020 by the authors. Licensee MDPI, Basel, Switzerland. This article is an open access article distributed under the terms and conditions of the Creative Commons Attribution (CC BY) license (<http://creativecommons.org/licenses/by/4.0/>).